Aerosol Effects on the Development of Cumulus Clouds over the Tibetan Plateau

Xu Zhou[1,5], Naifang Bei[2], Hongli Liu[3], Junji Cao[1], Li Xing[1], Wenfang Lei[4], Luisa T. Molina[4], and Guohui Li[1*]

[1]Key Lab of Aerosol Chemistry and Physics, SKLLQG, Institute of Earth Environment, Chinese Academy of Sciences, Xi'an, China
[2]School of Human Settlements and Civil Engineering, Xi'an Jiaotong University, Xi'an, Shaanxi, China
[3]State Key Laboratory of Severe Weather, Chinese Academy of Meteorological Sciences, Beijing, China
[4]Molina Center for Energy and the Environment, La Jolla, CA, USA
[5]University of Chinese Academy of Science, Beijing, China
[*]Correspondence to: Guohui Li (ligh@ieecas.cn)

Abstract. The aerosol-cloud interaction over the Tibetan Plateau has been investigated using a cloud-resolving weather research and forecasting model with a two-moment bulk microphysical scheme including aerosol effects on cloud condensation nuclei and ice nuclei. Two types of cumulus clouds with a similar convective available potential energy, occurring over the Tibetan Plateau (Cu-TP) and North China Plain (Cu-NCP) in August 2014, are simulated to explore the response of convective clouds to aerosols. A set of aerosol profiles is used in the simulations, with the surface aerosol number concentration varying from 20 to 9000 cm^{-3} and the sulfate mass concentration varying from 0.02 to 9.0 μg cm^{-3}. Increasing aerosol concentrations generally enhances the cloud core updraft and maximum updraft, intensifying convections in Cu-TP and Cu-NCP. However, the core updraft is much stronger in Cu-TP than Cu-NCP, because of the early occurrence of the glaciation process in Cu-TP that is triggered at an elevation above 4000 m. The precipitation increases steadily with aerosol concentrations in Cu-NCP, caused by the suppression of the warm rain but efficient mix-phased precipitation due to the reduced cloud droplet size. The precipitation in Cu-TP also increases with aerosol concentrations, but the precipitation enhancement is not substantial compared to that in Cu-NCP with high aerosol concentrations. The aerosol-induced intensification of convections in Cu-TP not only facilitates the precipitation, but also transports more ice-phase hydrometeors into the upper troposphere to decrease the precipitation efficiency. Considering the very clean atmosphere over the Tibetan Plateau, elevated aerosol concentrations can remarkably enhance convections due to its specific topography, which not only warms the middle troposphere to influence the Asian summer monsoon, but also delivers hydrometeors into the upper troposphere to allow more water vapor to travel into the lower stratosphere.

1 Introduction

Atmospheric aerosols, formed naturally and anthropogenically, influence the radiative energy budget of the Earth-atmosphere system in many ways. They scatter or absorb a fraction of the incoming solar radiation to cool or warm the atmosphere, decreasing surface temperature and altering atmospheric stability (e.g., Jacobson, 2002; Wang et al., 2013). They also serve as cloud condensation nuclei (CCN) and ice nuclei (IN), modifying optical properties and lifetime of clouds (e.g., Penner et al., 2001; Zhang et al., 2007). The aerosol indirect effect, generally referred to as the aerosol impact on cloud reflective properties and lifetime (Twomey, 1977; Houghton, 2001), has constituted one of the largest uncertainties in climate prediction (IPCC, 2013). In addition, the aerosol effects on precipitation have been regarded as an important but poorly understood process that could have major implications to climate and water supplies (Levin and Cotton, 2007; Wang et al., 2014a; b).

For a given amount of condensable water vapor, elevated aerosol concentrations increase the number of cloud droplets and reduce their sizes, enhancing not only the reflective properties but also the lifetime of clouds through suppressing warm rain processes (Twomey, 1977; Albrecht, 1989). Accumulative observational and modeling evidence has shown that reduced cloud droplet size, due to increasing CCN, inhibits collision and coalescence processes, suppressing warm rain and delaying the onset of precipitation. Therefore, more droplets are further allowed to be transported above the 0°C isotherm, triggering the efficient mixed-phase process to release more latent heat and intensify the convection (e.g. Rosenfeld and Lensky, 1998; Rosenfeld and Woodley, 2000; Kaufman and Nakajima, 1993; Andreae et al., 2004; Kaufman et al., 2005; Fan et al., 2007; Khain et al., 2008; Koren et al., 2010; Li et al., 2013; Loftus and Cotton, 2014). However, recent studies have shown that an optimal aerosol loading exists to invigorate convection (Rosenfeld et al., 2008; Koren et al., 2014; Dagan et al., 2015). Additionally, the aerosol impacts on cloud

63 developments are also proposed to be dependent on the environmental conditions, such as
64 relative humidity and vertical wind shear (van den Heever et al., 2007; Lee et al., 2008; Fan
65 et al., 2009; Tao et al., 2012; Fan et al., 2016).

66 The observational and model-derived evidence on how aerosols influence rainfall
67 remains elusive due to the complexity of cloud processes, which are determined by intricate
68 thermodynamic, dynamical, and microphysical processes and their interactions (Levin and
69 Cotton, 2007; McComiskey and Feingold, 2012; Lin et al., 2016). Observations have
70 demonstrated that the aerosol effect on precipitation depends on both the type of aerosols and
71 precipitating environments. Rainfall reduction has been observed in polluted industrial and
72 urban regions in shallow clouds or clouds with the top temperature exceeding -10°C (e.g.,
73 Rosenfeld, 2000; Ramanathan et al., 2001; Andreae et al., 2004; Yang et al., 2013). However,
74 documented rainfall increase has also been observed around heavily polluted coastal areas or
75 over oceans influenced by anthropogenic aerosols (e.g., Cerveny and Balling, 1998; Shepherd
76 and Burian, 2003; Zhang et al., 2007; Li et al., 2008b; Koren et al., 2012, 2014). Model
77 results tend to support the argument that increasing aerosol concentrations enhances
78 precipitation under a moist, unstable atmosphere (e.g., Khain et al., 2005; Fan et al., 2007; Li
79 et al., 2008a, 2009; Wang et al., 2011; Fan et al., 2013).

80 The Tibetan Plateau (TP), located in the central eastern Eurasia and with an average
81 elevation of more than 4000 m, significantly affects the formation and variability of the Asian
82 summer monsoon through mechanical and thermal dynamical effects (Wu et al., 2007). Due
83 to its strong surface heating, the cumulus clouds are active over the TP and can be organized
84 to form convective systems, contributing substantially to the precipitation over TP and
85 adjacent areas. The TP is surrounded by several important natural and anthropogenic aerosol
86 sources, and the in-situ and satellite measurements have shown that anthropogenic aerosols
87 and dust have been lofted to the TP, directly influencing the regional climate (Engling et al.,

2011). Soot aerosols deposited on the TP glaciers have been confirmed to contribute significantly to observed glacier retreat (Xu et al., 2009). Absorbing aerosols over the TP have been proposed to directly affect monsoon rainfall through the elevated heat pump mechanism (Lau et al., 2008; D'Errico et al., 2015; Li et al., 2016).

However, to date few studies have been performed to investigate the aerosol indirect effect or the aerosol-cloud interaction over the TP. In the present study, we report an investigation of the aerosol effect on the cumulus cloud development and precipitation over the TP. Two types of cumulus clouds occurring over the TP and the North China Plain (NCP) are simulated using a cloud-resolving weather research and forecasting model for comparisons. The model configuration is described in Section 2. The results and discussions are presented in Section 3, and summary and conclusions are given in Section 4.

2 Models and Design of Numerical Experiments

2.1 Model Configuration

A cloud-resolving weather research and forecasting (CR-WRF) model (Skamarock et al., 2004) is used in the study to simulate cumulus clouds. A two-moment bulk microphysical scheme developed by Li et al. (2008a) is utilized to account for the aerosol-cloud interactions in the simulations. The mass mixing ratio and number concentration of five hydrometeors are predicted in the bulk microphysical scheme, including cloud water, rain water, ice crystal, snow flake, and graupel. The gamma function is used to represent the size distribution of the five hydrometeors. Detailed information is provided in Li et al. (2008a).

In order to consider the aerosol activation to CCN and IN, the CMAQ/models3 aerosol module (Binkowski and Roselle, 2003) is implemented into the CR-WRF model. Aerosols are simulated in the CMAQ using a modal approach assuming that particles are represented by three superimposed log-normal size distributions. The aerosol species, including sulfate,

nitrate, ammonium, organic and black carbon, and other unidentified species (dust-like) are predicted in the module.

For the CCN nucleation, the critical radius of dry aerosols is calculated from the *k*-Köhler theory developed by Petters and Kreidenweis (2007; 2008; 2013) using water supersaturation predicted by the CR-WRF model (Roger and Yau, 1989; Pruppacher and Klett, 1997). If the activated CCN radius is less than 0.03 μm, the mass of water condensation on CCN is calculated under the equilibrium assumption; otherwise, the mass of water condensing on CCN is calculated by $m_w = K\frac{4}{3}\pi r_a^3 \rho_w$ at zero supersaturation, where $3 < K < 8$ (Khain et al., 2000). Additionally, a novel, flexible approach, proposed by Philips et al. (2008, 2013) has been used to parameterize the ice heterogeneous nucleation within clouds. The method has empirically derived dependencies on the chemistry and surface area of multiple species of IN aerosols, mainly including dust, black and organic carbon aerosols. Three kinds of ice nucleation mechanisms are considered in the method, including contact, immersion, and condensation freezing.

2.2 Design of Numerical Experiments and Statistical Method in Data Analysis

The spatial resolution used in the cloud simulations is 1 km in the horizontal direction and about 250 m in the vertical direction. The model domain of 200 × 200 × 80 grid boxes along the x, y, and z directions, respectively, has been used to provide 200 km × 200 km horizontal and 20-km vertical coverage in this study. The initial and boundary conditions of water vapor are from the sounding data. The simulations use the open boundary conditions under which variables of all horizontal gradients are zero at the lateral boundary.

Two types of cumulus clouds are simulated using the CR-WRF model. The cumulus cloud over the TP (hereafter referred to as Cu-TP) is initialized using the sounding data (87.08°E, 28.63°N, 4302 m a.s.l.) at 0800 UTC on August 24, 2014 (Figure 1a). The cumulus cloud over the NCP (hereafter referred to as Cu-NCP) is initialized using the sounding data

(114.35°E, 37.17°N, 181 m a.s.l.) at 0800 UTC on August 12, 2014 (Figure 1b). The selected sounding profiles over the TP and NCP reveal a moderate instability in the atmosphere, with similar convective available potential energy (CAPE) for comparison, i.e., 675 J kg^{-1} for Cu-TP and 651 J kg^{-1} for Cu-NCP. Although Cu-TP and Cu-NCP have the similar CAPE, the remarkable difference of the initialization elevation between Cu-TP and Cu-NCP causes their distinct development processes. The 0°C isotherm is generally at the level of around 5 km a.s.l. in the summer. Therefore, when an air parcel perturbed in the boundary layer ascends to form a cloud, the rising distance to the 0°C isotherm is around 1 km over the TP and about 4 km over the NCP. Therefore, the occurrence of the efficient mixed phase process is much earlier for the cumulus cloud over the TP than the NCP, which substantially advances the development of the cloud over the TP.

The cumulus development is triggered by a warm bubble 15-km wide and a maximum temperature anomaly of 4°C at the height of 1.5 km a.g.l. (Li et al., 2008a) and the integration time is two hours. Observed aerosol concentrations over the TP exhibit a large variation during the monsoon season, i.e., the observed sulfate concentrations range from 0.1 to several $\mu g\ m^{-3}$ (Decesari et al., 2010). Therefore, a set of 28 initial aerosol size distributions with the aerosol number concentration ranging from 20 to 9000 cm^{-3} and the sulfate mass concentration ranging from 0.02 to 9.0 $\mu g\ cm^{-3}$ at the surface level are used. Other aerosol species are scaled using the measurement at the Nepal Climate Observatory-Pyramid (NCO-P) (Decesari et al., 2010). These aerosol distributions are designated for environments ranging from very clean background air mass to polluted urban plumes over the TP and NCP. Although the observed organic aerosol dominates the aerosol composition at NCO-P (Decesari et al., 2010), considering the large uncertainties in the hygroscopicity of organic aerosols, the hygroscopicity parameter for the secondary organic aerosol is set to be 0.05 in the study (Petters and Kreidenweis, 2007; 2008). Hence, sulfate aerosols (or inorganic

aerosols) still play a dominant role in the CCN activation. The aerosol concentration is assumed to decrease exponentially with height in the model simulations (Li et al., 2008a).

We have adopted several assumptions and simplifications for the processes associated with aerosols. In the simulations, only the accumulation mode of aerosols is used for the CCN and IN activation, and the aerosol spatial distributions are determined by the initial and boundary conditions, without consideration of chemistry, emissions, and release from cloud droplet evaporation or ice crystal sublimation. The sulfate, nitrate, ammonium, black carbon, organic, and dust-like aerosols in the accumulation mode are included to consider the aerosol CCN and IN effects. Therefore, the surface-level aerosol number concentration ([*Na*]) is used to represent all types of aerosols, and the CCN concentration at a certain supersaturation (SS) is not used in the study. It is worth noting that the simple aerosol assumption is subject to cause rather large uncertainties in the aerosol activation to CCN and IN. Aerosol chemistry in clouds plays a considerable role in the aerosol nucleation and growth. Direct emissions from anthropogenic sources contribute substantially to the CCN and IN, even over the TP with increasing human activities. Furthermore, mineral dust from the natural source frequently dominates the TP throughout the year. Therefore, future studies need to be conducted to include all the aerosol modes, chemistry, and emissions.

In order to evaluate the overall response of simulated cumulus clouds to changes in aerosol concentrations, the population mean (p-mean) of a given variable over all qualified grid points and for a given integration interval is used in the study (Wang, 2005), defined as:

$$\bar{C}^{p} = \frac{1}{\sum_{t=T_1}^{T_2} N(t)} \sum_{t=T_1}^{T_2} \sum_{n>n_{min}}^{q>q_{min}} c(x, y, t)$$

where c represents a given quantity. The calculation only applies to the grid points where both the mass concentration q and number concentration n of a hydrometeor or the summation of several hydrometeors exceed the given minima. The total number of the grid

points at a given output time step t is represented by $N(t)$. T_1 and T_2 are the start and end output time steps, respectively.

3. Results and Discussions

3.1 Response of Cloud Properties to Changes in Aerosol Concentrations

Figure 2a depicts the dependence of the p-mean of the cloud droplet number concentration (CDNC) on the [*Na*]. Increasing [*Na*] provides more CCN to activate, and although more activated droplets compete for the available water vapor, the water vapor condensation efficiency is enhanced due to the increased bulk droplet surface area, accelerating the latent heat release and the updraft to provide more supersaturated water vapor. Therefore, the increasing CDNC is well consistent with increasing [*Na*] in Cu-TP and Cu-NCP, in good agreement with previous studies (e.g., Fan et al., 2007a, b; Li et al., 2008a). When the [*Na*] increases from about 20 cm^{-3} to 9000 cm^{-3}, the p-mean of the CDNC increases from 0.56 cm^{-3} to 218 cm^{-3} for Cu-NCP. However, more aerosols are activated in Cu-TP compared to Cu-NCP, and the p-mean of the CDNC increases from 0.80 cm^{-3} to 415 cm^{-3} for Cu-TP. Although the CAPE is similar for Cu-TP and Cu-NCP, the p-mean of CDNC in Cu-TP is higher than that in Cu-NCP with the same [*Na*].

With the [*Na*] increasing from 20 to 9000 cm^{-3}, the effective radius of cloud droplet (R_{eff}) in Cu-TP is reduced from about 18.5 to 4 .1 μm, and the R_{eff} in Cu-NCP is also consistently reduced from 14.3 to 6.6 μm (Figure 2b). Interestingly, when the [*Na*] is less than about 240 cm^{-3}, the R_{eff} in Cu-TP is larger than that in Cu-NCP with the same [*Na*], although the CDNC in Cu-TP is higher than that in Cu-NCP, showing more cloud water condensed in Cu-TP. Figure 3a presents the dependence of the cloud water content (CWC) on the [*Na*] in Cu-TP and Cu-NCP, showing that the CWC increases with increasing [*Na*]. This positive relationship is caused by the combined effects of the increase in CDNC and the

decrease in R_{eff}, which inhibit the collision/coalescence of cloud droplets and also enhance the water vapor condensation efficiency and the updraft to generate more available condensable water vapor. The CWC in Cu-TP is higher than that in Cu-NCP for the same [*Na*], due to higher CDNC and likely stronger updrafts in Cu-TP. The Cu-TP is triggered at an elevation of more than 4000 m a.s.l. Therefore, considering that the 0°C isotherm is at the level of around 5000 m a.s.l., the cloud water formed in the cumulus tends to be transported above the 0°C isotherm to become supercooled, initiating the efficient mixed phase process to release more latent heat and enhance the updraft. Therefore, there exists more supercooled cloud water in Cu-TP than Cu-NCP when [*Na*] are same (Figure 3b).

Figure 4 provides the vertical profiles of the hydrometeors mass concentrations (summed over the horizontal domain and then averaged during the simulation period) under three aerosol scenarios: a very low [*Na*] of 90 cm^{-3}, a low [*Na*] of 900 cm^{-3}, and a high [*Na*] of 9000 cm^{-3}, corresponding the background, clean, and polluted atmosphere, respectively. In Cu-TP and Cu-NCP, the CWC achieves the highest under the high [*Na*] case and the lowest under the very low [*Na*] case (Figures 4a and 4b). A higher [*Na*] enhances CDNC and reduces R_{eff}, suppressing the conversion from cloud water to rain water and sustaining more CWC in the cloud. In Table 1, the initial formation time of rain water is delayed with the [*Na*] increase in Cu-TP and Cu-NCP. The height of the maximum CWC slightly increases from the very low to high [*Na*] conditions in Cu-TP and Cu-NTP, but the maximum CWC occurs at 6~8 km a.s.l. in Cu-TP and 2~4 km a.s.l. in Cu-NCP. Therefore, for Cu-TP, most of cloud droplets are above the 0°C isotherm (about 5 km a.s.l.) and supercooled.

The ice particles (ice + snow) generally reach the highest in the high [*Na*] and lowest in the very low [*Na*], which is consistent with those of the CWC in Cu-TP and Cu-NCP (Figures 4e and 4f). In the present study, the homogeneous freezing and rime-splintering mechanisms (DeMott et al., 1994; Hallett and Mossop, 1974) are included for the ice nucleation. In

addition, the heterogeneous ice nucleation, including the contact, immersion, and condensation freezing, are all parameterized using the method proposed by Philips et al. (2008; 2013), and has considered the IN effect, depending not only on temperature and ice supersaturation, but also on the chemistry and surface area of multiple species of IN aerosols. The [*Na*] Enhancement generally suppresses the warm rain process to reduce the rain water, but provides more IN and supercooled CWC to accelerate the ice nucleation process. In addition, the rime-splintering mechanism also affects the ice particle profiles at the height with temperature ranging from -8°C and -3°C (Hallet and Mosssop, 1974). At the height of 6~8 km a.s.l. in Cu-TP and 4~6 km a.s.l. in Cu-NCP, the ice particles profiles are similar in the very low and low [*Na*] cases, which is caused by the rime-splintering mechanism. The ice crystal production from the rime-splintering mechanism is related to the graupel particles and the cloud droplets with radii exceeding 24 μm. Large cloud droplets in the very low [*Na*] facilitate the ice crystal productions from the rime-splintering mechanism, increasing the ice particles mass concentrations at the height of 6~8 km a.s.l. in Cu-TP and 4~6 km a.s.l. in Cu-NCP. Furthermore, there are more ice particles in Cu-TP than Cu-NCP with the same [*Na*] condition. The initial formation time of ice crystals is advanced by at least 12 minutes in Cu-TP compared to Cu-NCP (Table 1). The 0°C isotherm is at the level of around 5 km a.s.l. for the Cu-TP and Cu-NCP. However, the occurrence heights for the Cu-TP and Cu-NCP are more than 4 km and about 0.2 km a.s.l, respectively, and when an air parcel perturbed in the boundary layer ascends to form a cloud, the rising distance to the 0°C isotherm is about 1 km over the TP and around 4 km over the NCP. Therefore, the ice crystal formation time is significantly shortened in the Cu-TP compared to the Cu-NCP. The early formation of ice crystals not only facilitates their growth, also advances the glaciation process to intensify convections, further enhancing the growth process.

The rainwater in Cu-TP achieves the highest in the very low [*Na*] and lowest in the high [*Na*], and vice versa in Cu-NCP (Figures 4c and 4d). If not considering the contribution of graupel melting to the rainwater, enhancement of [*Na*] suppresses the warm rain process to reduce the rainwater, but enhances the raindrop size, which conversely accelerates the raindrop falling (Table 1). In Cu-TP, due to relatively low temperature below the freezing level and short falling distance (about 1 km), graupels dominate the precipitating particles, melting less to rainwater. So early occurrence of the warm rain process in the very low [*Na*] case causes the most rainwater formation (Figure 4c). However, in Cu-NCP, graupels falling below the freezing level tend to melt due to high temperature and long falling distance (about 4 ~ 5 km), enhancing the rainwater formation. More ice particles and supercooled CWC in the high [*Na*] case are favorable for the ice growth through deposition, aggregation among ice crystals, and riming of supercooled droplets (Wang and Change, 1993a, b; Lou et al., 2003), and heavily rimed ice crystals are transferred to graupels, enhancing the graupel formation. Therefore, in Cu-NCP, the high [*Na*] corresponds to the maximum graupel content and also rainwater content (Figures 4d and 4h). However, in Cu-TP, below 12 km, the low [*Na*] corresponds to the largest amounts of graupels. Early occurrence of the glaciation process in Cu-TP causes most of raindrops to be frozen to form graupels. The freezing rate of raindrops depends on the temperature, the raindrop size and number, and their corresponding variations with time (Lou et al., 2003). Generally, the raindrops with the larger size are easier to be frozen under the lower temperature. The [*Na*] Enhancement decreases the raindrop number, but increases its size and updraft to lower the temperature, causing the maximum raindrop freezing efficiency under the low [*Na*] condition. In addition, increasing the [Na] invigorates the convection and produce larger graupels, and then the melting of the graupel causes the formation of larger raindrops (Table 1).

285 It is worth noting that ice particles and graupels are transported above 12 km a.s.l. or
286 even exceeding 16 km a.s.l. (near tropopause) in Cu-TP, showing intensified convection and
287 also contributing to moistening the upper troposphere.

288 **3.2 Response of Convective Strength to Changes in Aerosol Concentrations**

289 The p-mean of the updraft and downdraft in a core area is used to measure the
290 convective strength of the simulated cumulus clouds, which is defined by the absolute
291 vertical wind speed exceeding 1 m s^{-1} and total condensed water mixing ratio more than 10^{-2}
292 g kg^{-1} (*Wang*, 2005). When the [*Na*] increases from 20 to 9000 cm^{-3}, the p-mean of the core
293 updraft increases from 2.0 to 4.3 m s^{-1} in Cu-TP, and from 1.5 to 2.7 m s^{-1} in Cu-NCP (Figure
294 5a). The enhancement of the core updraft with increasing [*Na*] is caused by the suppression
295 of the warm rain process to induce the more efficient mixed phase process, releasing more
296 latent heat to intensify the convection. With the same [*Na*], the p-mean of the core updraft is
297 larger in Cu-TP than in Cu-NCP, showing the significant impact of the early occurrence of
298 the glaciation process on the cloud development.

299 In Cu-TP, with the [*Na*] increase, the p-mean of the downdraft increases when the [*Na*]
300 is less than 90 cm^{-3}, but it becomes insensitive to the changes in [*Na*] when the [*Na*] is
301 between 90 and 1800 cm^{-3}, and commences to decrease when the [*Na*] exceeds 1800 cm^{-3}
302 (Figure 5b). The complex nonlinear variation of the p-mean of the downdraft with the [*Na*]
303 reflects the change in the vertical distribution of ice particles and graupels caused by the
304 enhancement of [*Na*] in Cu-TP. The enhancement of the convective strength with increasing
305 [*Na*] not only intensifies the convection to facilitate precipitation, producing more
306 precipitable particles, but also transports more ice particles and graupels to the upper
307 troposphere due to the specific topography and further suppress the occurrence of the
308 downdraft. However, the p-mean of the downdraft in Cu-NCP increases steadily with [*Na*].
309 Such an increase in the core downdraft with [*Na*] might be caused by the formation of a large

mass loading of precipitable particles to reduce buoyancy and increase downdrafts. Interestingly, when the [*Na*] is less than about 450 cm^{-3}, the p-mean of downdraft in Cu-TP is greater than that in Cu-NCP, but opposite when [*Na*] exceeding 450 cm^{-3}, indicating the influence of the early occurrence of the glaciation process due to the specific topography in Cu-TP.

The maximum updraft, representing the largest local latent heat release, generally increases with [*Na*] in Cu-TP and Cu-NCP (Figure 6a). The maximum updraft in Cu-TP is much higher than that in Cu-NCP with the same [*Na*]. In Cu-TP, when the [*Na*] exceeds 750 cm^{-3}, the maximum updraft becomes insensitive to changes in the [*Na*]. In Cu-NCP, the maximum updraft is not very sensitive to changes in the [*Na*] when the [*Na*] exceeds 2400 cm^{-3}. The maximum downdraft, or the largest drag speed, indicating the largest strength to inhibit the development of the convection, also increases generally with the [*Na*] in Cu-TP and Cu-NCP (Figure 6b), but Cu-TP produces the more intensive maximum downdraft than Cu-NCP.

3.3 Response of Precipitation to Changes in Aerosol Concentrations

Figure 7 shows the variation of the accumulated precipitation with [*Na*] in Cu-TP and Cu-NCP. Generally, the precipitation increases with [*Na*], which is consistent with previous modeling studies (e.g., Khain et al., 2005, 2008; Fan et al., 2007; Li et al., 2008a; 2009). Since Cu-TP and Cu-NCP occur under humid conditions, the precipitation enhancement with [*Na*] is also in good agreement with measurements. Observations have shown the precipitation enhancement around heavily polluted coastal urban areas (Shepherd and Burian, 2003; Ohashi and kida, 2002) or over oceans influenced by pollution aerosols (Cerveny and Balling, 1998; Li et al., 2008b; Koren et al., 2012, 2014).

When the [*Na*] is increased from about 20 cm^{-3} to 9000 cm^{-3}, the precipitation of Cu-TP increases from 0.13 mm to 0.23 mm; when the [*Na*] exceeds 300 cm^{-3}, the

335 precipitation becomes insensitive to the variation in [*Na*]. In contrast, the precipitation of
336 Cu-NCP consistently increases from 0.03 mm to 0.37 mm with [*Na*] ranging from 20 cm^{-3} to
337 9000 cm^{-3}. In addition, when the [*Na*] is less than 500 cm^{-3}, Cu-TP produces more
338 precipitation than Cu-NCP, which can be explained by the early occurrence of the glaciation
339 process causing less warm rain but more efficient mixed-phase processes. However, when the
340 [*Na*] exceeds 500 cm^{-3}, the precipitation efficiency of Cu-NCP is higher than that of Cu-TP,
341 although the convective strength is larger in Cu-TP than Cu-NCP. The increasing convective
342 strength with [*Na*] not only enhances the precipitation, but also transports more ice and
343 graupel particles above 12 km to form the anvil. The ice particles and grauples in the anvil
344 are subject to sublimation and evaporation to moisten the upper troposphere, and decrease the
345 precipitation efficiency in Cu-TP.

346 The water content and precipitation in the Cu-TP response well monotonically to the
347 changes in the [*Na*]. Numerous studies have shown that the reduced liquid water path (LWP)
348 by increasing aerosols under relatively dry conditions (e.g., Khain et al., 2005). During the
349 summer monsoon season, the atmosphere over the TP is humid due to the water vapor
350 transport by the monsoon (Figure 1a). The ambient humidity in the simulations of the Cu-TP
351 exceeds 80% in the low-level atmosphere, causing the good monotonicity in the responses of
352 water content and precipitation to aerosols.

353 **3.4 Sensitivity Studies**

354 Recent studies have demonstrated that convection is more active and stronger during
355 summertime over Tibetan Plateau due to its unique thermodynamic forcing (Hu et al., 2016).
356 We have further performed sensitivity studies to explore the impact of the maximum
357 perturbation temperature (MPT) in the warm bubble on the development of cumulus clouds.
358 The MPTs of 2.0°C and 0.5°C are used to trigger Cu-TP and Cu-NCP with the [*Na*] ranging
359 from 20 cm^{-3} to 9000 cm^{-3}.

For Cu-TP, the core updraft decreases slightly when the MPT is reduced from 4.0°C to 2.0°C, particularly when the [*Na*] exceeds 100 cm^{-3}, the decrease of the core updraft is indiscernible. When the MPT is reduced from 2.0°C to 0.5°C, the core updraft decreases considerably. However, for Cu-NCP, the core updraft decreases substantially when the MPT is reduced from 4.0°C to 0.5°C. When the MPT is 0.5°C and the [*Na*] is less than 80 cm^{-3}, the updraft core area is not formed in Cu-NCP. When the MPT is the same, the core updraft is much larger in Cu-TP than Cu-NCP with the same [*Na*]; even the core updraft in Cu-TP with the MPT of 0.5°C is larger than that in Cu-NCP with the MPT of 4.0°C when the [*Na*] is more than 80 cm^{-3}. Therefore, under the unstable conditions over the Tibetan Plateau, a small perturbation can induce strong convections, which is primarily caused by early occurrence of the glaciation process due to the specific topography, as discussed in Section 3.1.

The accumulated precipitation generally decreases with the MPT in Cu-TP and Cu-NCP with the same [*Na*]. When the MPT is 4.0°C, Cu-NCP produces more precipitation than Cu-TP with the [*Na*] exceeding 500 cm^{-3}, but Cu-TP produces much more precipitation than Cu-NCP with the MPT of 0.5°C under all aerosol conditions. In addition, the precipitation generally increases with increasing the [*Na*] in Cu-TP and Cu-NCP with various MPTs, and does not exhibit a nonlinear variation with the [*Na*], which is not consistent with the results in Li et al. (2008a). The possible reason is that in this study, the maximum p-mean of CDNC is about 410 cm^{-3}, which is much less than that in Li et al. (2008a). If the [*Na*] is further increased, the precipitation might be suppressed.

4. Summary and Conclusions

The aerosol-cloud interaction over the TP has been examined using the CR-WRF model with a two moment microphysical scheme considering the aerosol effects on CCN and IN. For comparisons, two types of cumulus clouds, occurring over the TP and NCP in August

2014, are modeled to examine the response of the cumulus clouds development to the change in aerosol concentrations. A set of 28 aerosol profiles are utilized in simulations, with the surface aerosol number concentration varying from 20 to 9000 cm^{-3} and the sulfate mass concentration varying from 0.02 to 9.0 μg cm^{-3}. Multiple aerosol species are considered to provide CCN and IN, including sulfate, nitrate, ammonium, organic and black carbon, and dust-like aerosols.

In general, with varying aerosol concentrations from very clean background condition to the polluted condition, more aerosols are activated, significantly increasing the CDNC and decreasing the droplet size in Cu-TP and Cu-NCP. Formation of a large amount of cloud droplets with small sizes suppresses the warm rain process and enhances water vapor condensation efficiency and updraft to generate more available condensable water vapor. When more cloud droplets are transported above the 0°C isotherm, occurrence of the mixed-phase process releases more latent heat to further enhance the cloud core updraft and increase precipitation, intensifying the convections in Cu-TP and Cu-NCP.

However, early occurrence of the glaciation process in Cu-TP, which is triggered at an elevation of more than 4000 m, causes large differences between Cu-TP and Cu-NCP. Much more supercooled cloud droplets are formed in Cu-TP than Cu-NCP with the same aerosol concentration, facilitating the mixed-phase process and significantly enhancing the core updraft and maximum updraft in Cu-TP compared to Cu-NCP. Nevertheless, the intensified convection induced by the increase of aerosol concentrations in Cu-TP not only facilitates the precipitation, but also delivers more ice-phase hydrometeors into the upper troposphere to form the anvil, decreasing the precipitation efficiency. Therefore, in Cu-TP, when aerosol concentrations are high, the precipitation enhancement becomes insignificant with increasing aerosol concentrations, but a considerable amount of ice-phase hydrometeors are lofted above 12 km or even exceeding 16 km. Additionally, sensitivity studies have also shown that under

410 the unstable conditions over the TP, a small perturbation in temperature can induce strong
411 convections, which is primarily caused by early occurrence of the glaciation process due to
412 the specific topography.

413 In the present study, both CCN and IN effects are considered in the cloud simulations.
414 However, there are still difficulties in quantitatively distinguish those two effects on the
415 ice-phase cloud development using sensitivity studies. Obviously, the CCN plays a dominant
416 role in the mixed-phase cloud development. Even when the IN is scare in the atmosphere, the
417 mixed-phase cloud development is not hindered with sufficient CCN, because freezing of
418 raindrops, the subsequent splinter-riming process, and homogeneous freezing of cloud
419 droplets still initialize the glaciation process to facilitate the development of the mixed phase
420 cloud.

421 It is worth noting that, although the CAPE is similar for the Cu-TP and Cu-NCP, it
422 might not be fair to compare aerosol impacts on the cloud development over the TP with the
423 NCP, considering the difference of the water vapor profile, wind shear, topography, and
424 anthropogenic and natural aerosol sources between the two regions. However, the
425 comparisons have highlighted that the topography plays a large role in the development of
426 cumulus over the TP.

427 Rapid growth of industrialization, urbanization, and transportation in Asia has caused
428 severe air pollution, progressively increasing aerosol concentrations in the regions
429 surrounding TP. Pollution aerosols from surrounding areas have been observed to be
430 transported to the TP. Considering the very clean atmosphere over the TP, elevated aerosol
431 concentrations can considerably enhance the convections due to its specific topography.
432 Numerous studies have shown that the TP significantly influences the formation and
433 variability of the Asian summer monsoon through mechanical and thermal dynamical effects
434 (e.g., Wu et al., 2007). In addition, Fu et al. (2006) have reported that convection over the TP

provides the main pathway for cross-tropopause transport in the Asian monsoon/TP region. Hence, intensification of convections due to the increase of aerosol concentrations over the TP not only enhances the latent heat release to warm the middle troposphere, influencing the Asian summer monsoon, also delivers more hydrometeors into the upper troposphere, allowing more water vapor to travel into the lower stratosphere. Further studies are needed to evaluate the aerosol indirect effect on the Asian summer monsoon and the troposphere/stratosphere exchange over the TP.

Acknowledgements. This work was supported by the National Natural Science Foundation of China (No. 41275153) and by the "Hundred Talents Program" of the Chinese Academy of Sciences. Naifang Bei is supported by the National Natural Science Foundation of China (No. 41275101). Luisa Molina and Wenfang Lei acknowledge support from US NSF Award 1560494.

Reference

Andreae, M. O., Rosenfeld, D., Artaxo, P., Costa, A. A., Frank, G. P., Longo, K. M., and Silva-Dias, M. A. F.: Smoking rain clouds over the Amazon, Science, 303, 1337–1342, 2004.

Binkowski, F. S. and Roselle, S. J.: Models-3 Community Multiscale Air Quality (CMAQ) model aerosol component 1. Model description, J. Geophys. Res., 108, 4183, doi:10.1029/2001JD001409, 2003.

Cerveny, R. S. and Bailing Jr., R. C.: Weekly cycles of air pollutants, precipitation and tropical cyclones in the coastal NW Atlantic region, Nature, 394, 561–563, 1998.

Dagan, G., Koren, I., and Altaratz, O.: Aerosol effects on the timing of warm rain processes, Geophys. Res. Lett., 42, 4590–4598, doi:10.1002/2015GL063839, 2015.

Decesari, S., Facchini, M. C., Carbone, C., Giulianelli, L., Rinaldi, M., Finessi, E., Fuzzi, S., Marinoni, A., Cristofanelli, P., Duchi, R., Bonasoni, P., Vuillermoz, E., Cozic, J., Jaffrezo, J. L., and Laj, P.: Chemical composition of PM_{10} and PM_1 at the high-altitude Himalayan station Nepal Climate Observatory-Pyramid (NCO-P) (5079 m a.s.l.), Atmos. Chem. Phys., 10, 4583–4596, doi:10.5194/acp-10-4583-2010, 2010.

DeMott, P. J., Meyers, M. P., and Cotton, W. R.: Parameterization and impact of ice initiation processes relevant to numerical model simulations of cirrus clouds, J. Atmos. Sci., 51, 77–90, doi:10.1175/1520-0469(1994)051<0077:paioii> 2.0.co;2, 1994.

D'Errico, M., Cagnazzo, C., Gogli, P. G., Lau, K. M., Von, H. J., Fierli, F., and Cherchi, A.: Indian monsoon and the elevated-heat pump mechanism in a coupled aerosol-climate model, J. Geophys. Res., 120, 8712–8723, doi: 10.1002/2015JD023346, 2015.

Engling, G., Zhang, Y.-N., Chan, C.-Y., Sang, X.-F., Lin, M., Ho, K.-F., Li, Y.-S., Lin, C.-Y., and Lee, J. J.: Characterization and sources of aerosol particles over the southeastern Tibetan Plateau during the Southeast Asia biomass-burning season, Tellus B, 63, 117–128, doi:10.1111/j.1600-0889.2010.00512.x, 2011.

Fan, J., Leung, L. R., Rosenfeld, D., Chen, Q., Li, Z. Q., Zhang, J. Q., and Yan, H. R.: Microphysical effects determine macrophysical response for aerosol impacts on deep convective clouds, P. Natl. Acad. Sci. USA, 110, E4581–E4590, doi:10.1073/pnas.1316830110, 2013.

Fan, J., Wang, Y., Rosenfeld, D., and Liu, X.: Review of aerosol-cloud interactions: Mechanisms, significance, and challenges, *J. Atmos. Sci*., *73*, 4221–4252, 2016.

Fan, J., Yuan, T. L., Comstock, J. M., Ghan, S., Khain, A., Leung, L. R., Li, Z. Q., Martins, V. J., and Ovchinnikov, M.: Dominant role by vertical wind shear in regulating aerosol effects on deep convective clouds, J. Geophys. Res., 114, D22206, doi:10.1029/2009jd012352, 2009.

Fan, J., Zhang, R., Li, G., Tao, W.-K and Li, X.: Simulations of cumulus clouds using a spectral microphysics cloud-resolving model, J. Geophys. Res., 112, D04201, doi:10.1029/2006JD007688, 2007a.

Fan, J., Zhang, R., Li, G., and Tao, W.-K.: Effects of aerosols and relative humidity on cumulus clouds, J. Geophys. Res., 112, D14204, doi:10.1029/2006JD008136, 2007b.

Fu, R., Hu, Y., Wright, J. S., Jiang, J. H., Dickinson, R. E., Chen, M., Filipiak, M., Read, W. G., Waters, J. W., and Wu, D. L.: Short circuit of water vapor and polluted air to the

492 global stratosphere by convective transport over the Tibetan Plateau, P. Natl. Acad. Sci.
493 USA, 103, 5664–5669, doi:10.1073/pnas.0601584103, 2006.

494 Hallett, J. and Mossop, S. C.: Production of secondary ice crystals during the riming process,
495 Nature, 249, 26–28, 1974.

496 Houghton J.: The science of global warming, Interdiscip. Sci. Rev., 26, 247–257,
497 doi:10.1179/030801801679485, 2001.

498 Hu, L., Deng, D., Gao, S., and Xu, X.: The seasonal variation of Tibetan Convective Systems:
499 Satellite observation, J. Geophys. Res., 121, doi:10.1002/2015JD024390, 5512–5525,
500 2016.

501 IPCC: Summary for Policymakers, in: Climate Change 2013: The Physical Science Basis.
502 Contribution of Working Group I to the Fifth Assessment Report of the
503 Intergovernmental Panel on Climate Change, edited by: Stocker, T. F., Qin, D., Plattner,
504 G.-K., Tignor, M., Allen, S. K., Boschung, J., Nauels, A., Xia, Y., Bex, V., and Midgley,
505 P. M., Cambridge University Press, Cambridge, UK and New York, NY, USA, 2013.

506 Jacobson, M. Z.: Analysis of aerosol interactions with numerical techniques for solving
507 coagulation, nucleation, condensation, dissolution, and reversible chemistry among
508 multiple size distributions, J. Geophys. Res., 107, 4366, doi:10.1029/2001JD002044,
509 2002.

510 Kaufman, Y. J. and Nakajima, T.: Effect of Amazon smoke on cloud microphysics and
511 albedo – Analysis from satellite imagery, J. Appl. Meteor., 32, 729–744, 1993.

512 Kaufman, Y. J., Koren, I., Remer, L. A., Rosenfeld, D., and Rudich, Y.: The effect of smoke,
513 dust, and pollution aerosol on shallow cloud development over the Atlantic Ocean, P.
514 Natl. Acad. Sci. USA, 102, 11207–11212, doi:10.1073/pnas.0505191102, 2005.

515 Khain, A. P.: Notes on state-of-art investigations of aerosol effects on precipitation: a critical
516 review, Environ. Res. Lett., 4, 015004, doi:10.1088/1748-9326/4/1/015004, 2000.

517 Khain, A. P., BenMoshe, N., and Pokrovsky, A.: Factors determining the impact of aerosols
518 on surface precipitation from clouds: An attempt at classification, J. Atmos. Sci., 65,
519 1721–1748, doi:10.1175/2007jas2515.1, 2008.

520 Khain, A., Rosenfeld, D., and Pokrovsky, A.: Aerosol impact on the dynamics and
521 microphysics of deep convective clouds, Q. J. Roy. Meteor. Soc., 131, 2639–2663,
522 doi:10.1256/Qj.04.62, 2005.

523 Koren, I., Altaratz, O., Remer, L. A., Feingold, G., Martins, J. V., and Heiblum, R. H.:
524 Aerosol-induced intensification of rain from the tropics to the mid-latitudes, Nat. Geosci.,
525 5, 118–122, doi:10.1038/NGEO1364, 2012.

526 Koren, I., Dagan, G., and Altaratz, O.: From aerosol-limited to invigoration of warm
527 convective clouds, Science, 344, 1143–1146, doi:10.1126/science.1252595, 2014.

528 Koren, I., Remer, L. A., Altaratz, O., Martins, J. V., and Davidi, A.: Aerosol-induced changes
529 of convective cloud anvils produce strong climate warming, Atmos. Chem. Phys., 10,
530 5001–5010, doi:10.5194/acp-10-5001-2010, 2010.

531 Lau, K.-M., Tsay, S. C., Hsu, C., Chin, M., Ramanathan, V., Wu, G.-X., Li, Z., Sikka, R.,
532 Holben, B., Lu, D., Chen, H., Tartari, G., Koudelova, P., Ma, Y., Huang, J., Taniguchi, K.,
533 and Zhang, R.: The joint aerosol-monsoon experiment: A new challenge for Monsoon
534 Climate Research, B. Am. Meteorol. Soc., 89, 369–383, 2008.

Lee, S. S., Donner, L. J., Phillips, V. T. J., and Ming, Y.: The dependence of aerosol effects on clouds and precipitation on cloud-system organization, shear and stability, J. Geophys. Res., 113, D16202, doi:10.1029/2007jd009224, 2008.

Levin, Z. and Cotton, W.: Aerosol pollution impact on precipitation: A scientific review, World Meteorological Organization, Geneva, Switzerland, 2007.

Li, G., Wang, Y., and Zhang, R. Y.: Implementation of a two- moment bulk microphysics scheme to the WRF model to investigate aerosol-cloud interaction, J. Geophys. Res., 113, D15211, doi:10.1029/2007jd009361, 2008a.

Li, G., Wang, Y., Lee, K.-H., Diao, Y., and Zhang, R.: Increased winter precipitation over the North Pacific from 1984 – 1994 to 1995 – 2005 inferred from the Global Precipitation Climatology Project, Geophys. Res. Lett., 35, L13821, doi:10.1029/2008GL034668, 2008b.

Li, G., Wang, Y., Lee, K.-H., Diao, Y., and Zhang, R.: Impacts of aerosols on the development and precipitation of a mesoscale squall line, J. Geophys. Res., 114, D17205, doi:10.1029/2008JD011581, 2009.

Li, L., Hong, Y., Wang, J., Adler, R. F., Pollcelli, F. S., Habib, S., Irwn, D., Korme, T., and Okello, L.: Evaluation of the real-time TRMM-based multi-satellite precipitation analysis for an operational flood prediction system in Nzoia Basin, Lake Victoria, Africa, Nat. Hazards, 50, 109, doi:10.1007/s11069-008-9324-5, 2009.

Li, X., Tao, W.-K., Masunaga, H., Gu, G., and Zeng , X.: Aerosol effects on cumulus congestus population over the tropical Pacific: Cloud resolving modeling study, J. Meteorol. Soc. Jpn., 91, 817–833, 2013.

Li, Z., Lau, W. K.-M., Ramanathan, V., Wu, G., Ding, Y., Manoj, M. G, Liu, J., Qian, Y., Li, J., Zhou, T, Fan, J., Rosenfeld, D, Ming, Y, Wang, Y., Huang, J, Wang, B., Xu, X., Lee, S.-S. Cribb, M., Zhang, F., Yang, X., Zhao, C., Takemura, T., Wang, K., Xia, X., Yin, Y., Zhang, H, Guo, J., Zhai, P. M. Zhai, Sugimoto, N., Babu, S. S., and Brasseur, G. P.: Aerosol and monsoon climate interactions over Asia, Rev. Geophys., 54, 866–929, 2016.

Lin, Y., Wang, Y., Pan, B., Hu, J., Liu, Y., and Zhang, R.: Distinct impacts of aerosols on an evolving continental cloud complex during the RACORO field campaign, J. Atmos. Sci., 73, 3681–3700, 2016.

Loftus, A.M., and Cotton, W.R.: Examination of CCN impacts on hail in a simulated supercell storm with triple-moment hail bulk microphysics, Atmos. Res., s147–148(1), 183–204, 2014.

Lou, X.-F., Hu, Z.-J., and Shi, Y.-Q.: Numerical simulation of a heavy rainfall case in South China, Adv. Atmos. Sci., 20, 128–138, 2003.

McComiskey, A. and Feingold, G.: The scale problem in quantifying aerosol indirect effects, Atmos. Chem. Phys., 12, 1031-1049, doi:10.5194/acp-12-1031-2012, 2012.

Ohashi, Y. and Kida, H.: Local circulations developed in the vicinity of both coastal and inland urban areas: A numerical study with a mesoscale atmospheric model, J. Appl. Meteor., 41(1), 30–45, 2002.

Penner, J. E., Hegg, D., and Leaitch, R.: Unraveling the role of aerosols in climate change, Environ. Sci. Technol., 35, 332–340, 2001.

Petters, M. D. and Kreidenweis, S. M.: A single parameter representation of hygroscopic growth and cloud condensation nucleus activity, Atmos. Chem. Phys., 7, 1961–1971,

579 doi:10.5194/acp-7-1961-2007, 2007.

580 Petters, M. D. and Kreidenweis, S. M.: A single parameter representation of hygroscopic
581 growth and cloud condensation nucleus activity – Part 2: Including solubility, Atmos.
582 Chem. Phys., 8, 6273–6279, doi:10.5194/acp-8-6273-2008, 2008.

583 Petters, M. D. and Kreidenweis, S. M.: A single parameter representation of hygroscopic
584 growth and cloud condensation nucleus activity – Part 3: Including surfactant partitioning,
585 Atmos. Chem. Phys., 13, 1081–1091, doi:10.5194/acp-13-1081-2013, 2013.

586 Phillips, T. J., DeMott, P. J., and Andronache, C.: An empirical parameterization of
587 heterogeneous ice nucleation for multiple chemical species of aerosol, J. Atmos. Sci., 65,
588 2757–2783, 2008.

589 Phillips, T. J., DeMott, P. J., Andronache, C., Pratt, K. A., Prather, K. A., Subramanian, R.,
590 and Twohy, C.: Improvements to an empirical parameterization of heterogeneous ice
591 nucleation and its comparison with observations, 70, 378–408, 2013.

592 Pruppacher, H. R. and Klett, J. D.: Microphysics of clouds and precipitation, second revised
593 and enlarged edition with an introduction to cloud chemistry and cloud electricity,
594 Kluwer Academic Publishers, Reidel, Dordrecht, 954 pp., 1997.

595 Ramanathan. V., Crutzen, P. J., Kiehl, J. T., and Rosenfeld, D.: Aerosols, climate, and the
596 hydrological cycle, Science, 294, 2119–2124, 2001.

597 Rogers, R. R. and Yau, M. K.: A short course in cloud physics, Pergamon, Tarrytown, New
598 York, 1989.

599 Rosenfeld, D.: Suppression of rain and snow by urban and industrial air pollution, Science,
600 287, 1793–1796, 2000.

601 Rosenfeld, D. and Lensky, I. M.: Satellite-based insights into precipitation formation
602 processes in continental and maritime convective clouds, B. Am. Meteorol. Soc., 79,
603 2457–2476, 1998.

604 Rosenfeld, D., and Woodley, W. L.: Deep convective clouds with sustained supercooled
605 liquid water down to -37.5 C, Nature, 405, 440–442, 2000.

606 Rosenfeld, D., Lohmann, U., Raga, G. B., O'Dowd, C. D., Kulmala, M., Fuzzi, S., Reissell,
607 A., and Andreae, M. O.: Flood or drought: how do aerosols affect precipitation?, Science,
608 321, 1309–1313, 2008.

609 Shepherd, J. M., and Burian, S. J.: Detection of urban-induced rainfall anomalies in a major
610 coastal city, Earth Interact., 7, 1–14,
611 doi:10.1175/1087-3562(2003)007<0001:DOUIRA>2.0.CO;2, 2003.

612 Skamarock, W. C.: Evaluating mesoscale NWP models using kinetic energy spectra, Mon.
613 Weather Rev., 132, 3019–3032, 2004.

614 Tao, W. K., Li, X. W., Khain, A., Matsui, T., Lang, S., and Simpson, J.: Role of atmospheric
615 aerosol concentration on deep convective precipitation: Cloud-resolving model
616 simulations, J. Geophys. Res., 112, D24S18, doi:10.1029/2007jd008728, 2007.

617 Tao, W. K., Chen, J. P., Li, Z., Wang, C., and Zhang, C.: Impact of aerosols on convective
618 clouds and precipitation, Rev. Geophys., 50, doi: 10.1029/2011RG000369, 2012.

619 Twomey, S. A.: The influence of pollution on the shortwave albedo of clouds, J. Atmos. Sci.,
620 34, 1149–1152, 1977.

Van Den Heever, S. C. and Cotton, W. R.: Urban aerosol impacts on downwind convective storms, J. Appl. Meteorol. Clim., 46, 828–850, doi:10.1175/JAM2492.1, 2007.

Wang, C. and Chang, J.: Three-dimensional numerical model of cloud dynamics, microphysics, and chemistry 1. Concepts and formulation, J. Geophys. Res., 98(D8), 14 827–14 844, 1993a.

Wang, C. and Chang, J.: Three-dimensional numerical model of cloud dynamics, microphysics, and chemistry 2. A case study of the dynamics and microphysics of a severe local storm, J. Geophys. Res., 98(D8), 14,845–14,862, 1993b.

Wang, C.: A modeling study of the response of tropical deep convection to the increase of cloud condensation nuclei concentration, 1. Dynamics and microphysics, J. Geophys. Res., 110, D21211, doi:10.1029/2004JD005720, 2005.

Wang, Y., Wan, Q., Meng, W., Liao, F., Tan, H., and Zhang, R.: Long-term impacts of aerosols on precipitation and lightning over the Pearl River Delta megacity area in China, Atmos. Chem. Phys., 11, 12421–12436, 2011.

Wang, Y., Khalizov, A., Levy, M., and Zhang, R.: New directions: Light absorbing aerosols and their atmospheric impacts", Atmos. Environ., 81, 713–715, 2013.

Wang, Y., Wang, M., Zhang, R., Ghan, S. J., Lin, Y., Hu, J., Pan, B., Levy, M., Jiang, J., and Molina, M. J.: Assessing the effects of anthropogenic aerosols on Pacific storm track using a multi-scale global climate mode, Proc. Natl Acad. Sci. USA, 111(19), 6894–6899, 2014a.

Wang, Y., Zhang, R., and Saravanan, R.: Asian pollution climatically modulates mid-latitude cyclones following hierarchical modelling and observational analysis, Nature Comm., 5, 3098, 2014b.

Wu, G., Liu, Y., Zhang, Q., Duan, A., Wang, T., Wan, R., Liu, X., Li, W., Wang, Z., and Liang, X.: The influence of mechanical and thermal forcing by the Tibetan Plateau on Asian climate, J. Hydrometeorol., 8, 770–789, doi:10.1175/JHM609.1, 2007.

Xu, B., Cao, J., Hansen, J., Yao, T., Joswia, D. R., Wang, N., Wu, G., Wang, M., Zhao, H., and Yang, W.: Black soot and the survival of Tibetan glaciers, P. Natl. Acad. Sci. USA, 106, 22114–22118, doi:10.1073/pnas.0910444106, 2009.

Yang, X., Ferrat, M. and Li, Z.: New evidence of orographic precipitation suppression by aerosols in central China, Meteorol. Atmos. Phys., 119,17–29, doi:10.1007/s00703-012-0221-9, 2013.

Zhang, R. Y., Li, G. H., Fan, J. W., Wu, D. L., and Molina, M. J.: Intensification of Pacific storm track linked to Asian pollution, P. Natl. Acad. Sci. USA, 104, 5295–5299, 2007.

Table 1 Response of cloud properties in Cu-TP and Cu-NCP under three aerosol conditions*.

Clouds	Cu-TP			Cu-NCP		
	Background	Clean	Polluted	Background	Clean	Polluted
Initial formation time of hydrometeors (minutes)						
Rain	10	14	20	8	10	14
Ice crystal	12	10	8	24	24	26
Graupel	12	14	16	18	18	16
P-mean of effective radius of hydrometeors (μm)						
Rain	119	132	647	110	151	223
Graupel	559	665	917	221	303	447

*The aerosol concentrations are 90, 900, and 9000 cm^{-3} for the background, clean, and polluted conditions, respectively.

Figure Captions

Figure 1 Atmospheric sounding (a) over the Tibetan Plateau (87.08°E, 28.63°N, 4302 m a.s.l.) at 0800 UTC on August 12, 2014 and (b) over North China Plain (114.35°E, 37.17°N, 181 m a.s.l.) at 0800 UTC on August 24, 2014. The black line corresponds to the temperature, and the blue line represents the dew point temperature.

Figure 2 Modeled p-mean of (a) cloud droplet number concentration and (b) effective radius as a function of the initial [N_a] in Cu-TP and Cu-NCP.

Figure 3 Modeled p-mean of (a) cloud water mass concentration and (b) supercooled cloud water mass concentration as a function of the initial [N_a] in Cu-TP and Cu-NCP in Cu-TP and Cu-NCP.

Figure 4 Vertical profiles of time-averaged masses of hydrometeors under background (90 cm^{-3}, blue), clean (900 cm^{-3}, green), and polluted (9000 cm^{-3}, red) [N_a] for (a) and (b) cloud water, (c) and (d) rain water, (e) and (f) ice particles (ice + snow), and (g) and (h) graupel in Cu-TP and Cu-NCP, respectively. The brown solid and dotted lines represent the surface level and the 0°C isotherm, respectively.

Figure 5 Simulated p-mean of (a) updraft and (b) downdraft in the core area (defined as an area where the absolute vertical velocity of wind is greater than 1 m s^{-1} and the total condensed water content exceeds 10^{-2} g kg^{-1}) as a function of the initial [N_a] in Cu-TP and Cu-NCP.

Figure 6 Modeled (a) maximum updraft and (b) minimum downdraft as a function of the initial [N_a] in Cu-TP and Cu-NCP.

Figure 7 Modeled cumulative precipitation inside the model domain (mm) as a function of the initial [N_a] in Cu-TP and Cu-NCP.

Figure 8 Response of (a) the p-mean of core updraft and (b) cumulative precipitation inside the model domain to the change in the maximum perturbation temperature of the warm bubble under various aerosol conditions in Cu-TP and Cu-NCP.

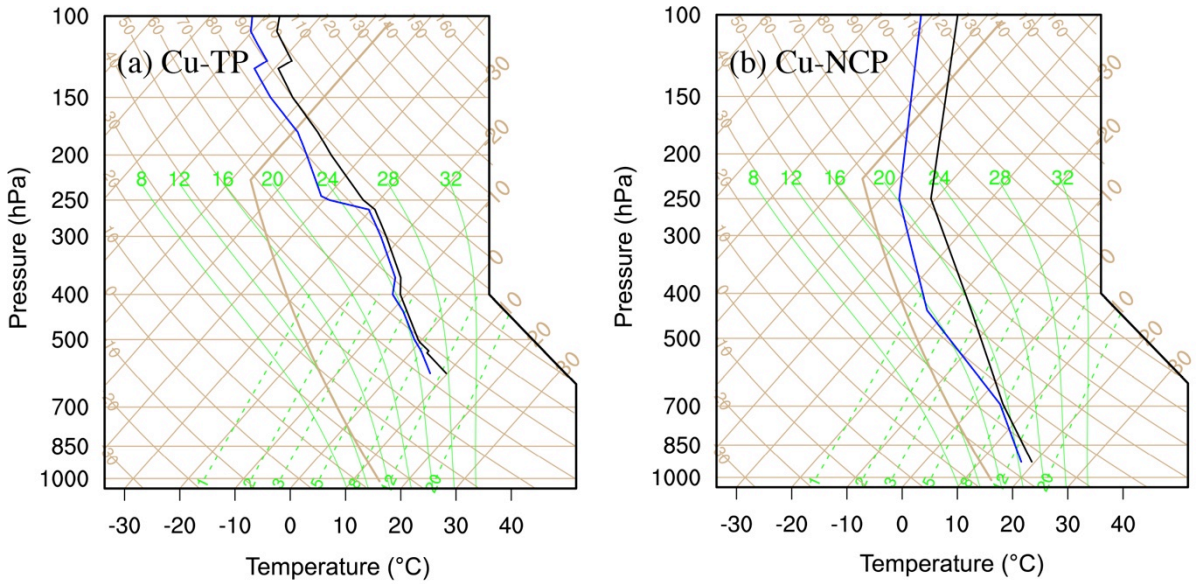

Figure 1 Atmospheric sounding (a) over the Tibetan Plateau (87.08°E, 28.63°N, 4302 m a.s.l.) at 0800 UTC on August 12, 2014 and (b) over North China Plain (114.35°E, 37.17°N, 181 m a.s.l.) at 0800 UTC on August 24, 2014. The black line corresponds to the temperature, and the blue line represents the dew point temperature.

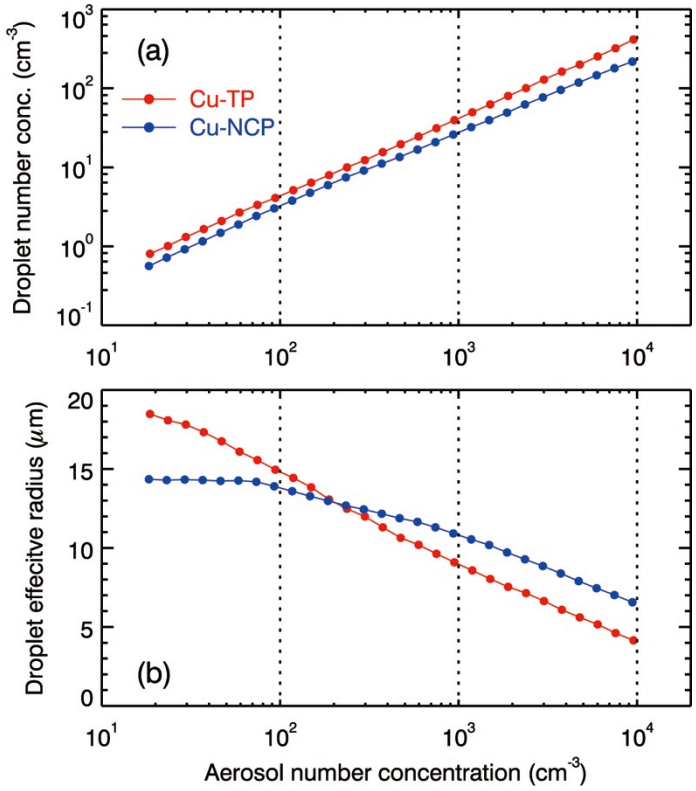

Figure 2 Modeled p-mean of (a) cloud droplet number concentration and (b) effective radius as a function of the initial [N_a] in Cu-TP and Cu-NCP.

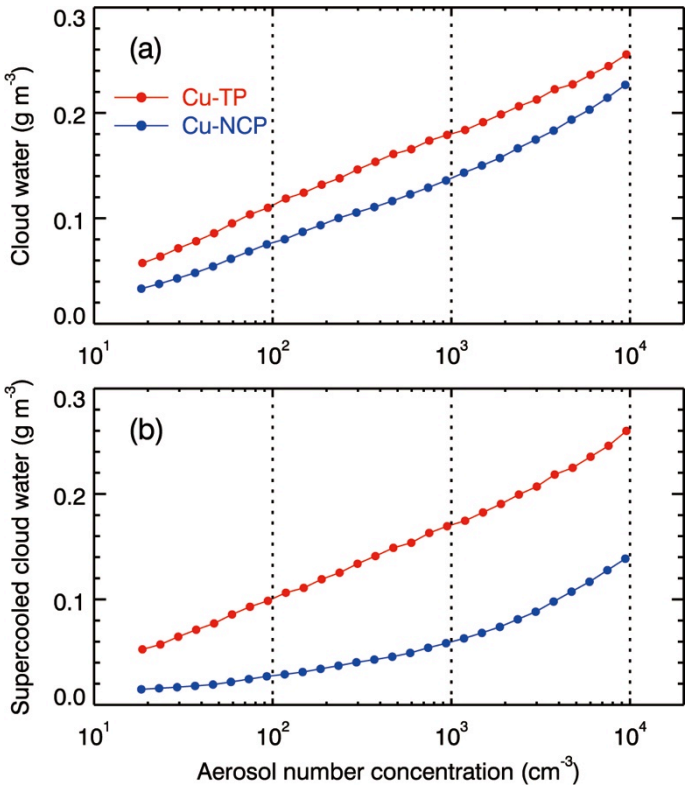

Figure 3 Modeled p-mean of (a) cloud water mass concentration and (b) supercooled cloud water mass concentration as a function of the initial [N_a] in Cu-TP and Cu-NCP in Cu-TP and Cu-NCP.

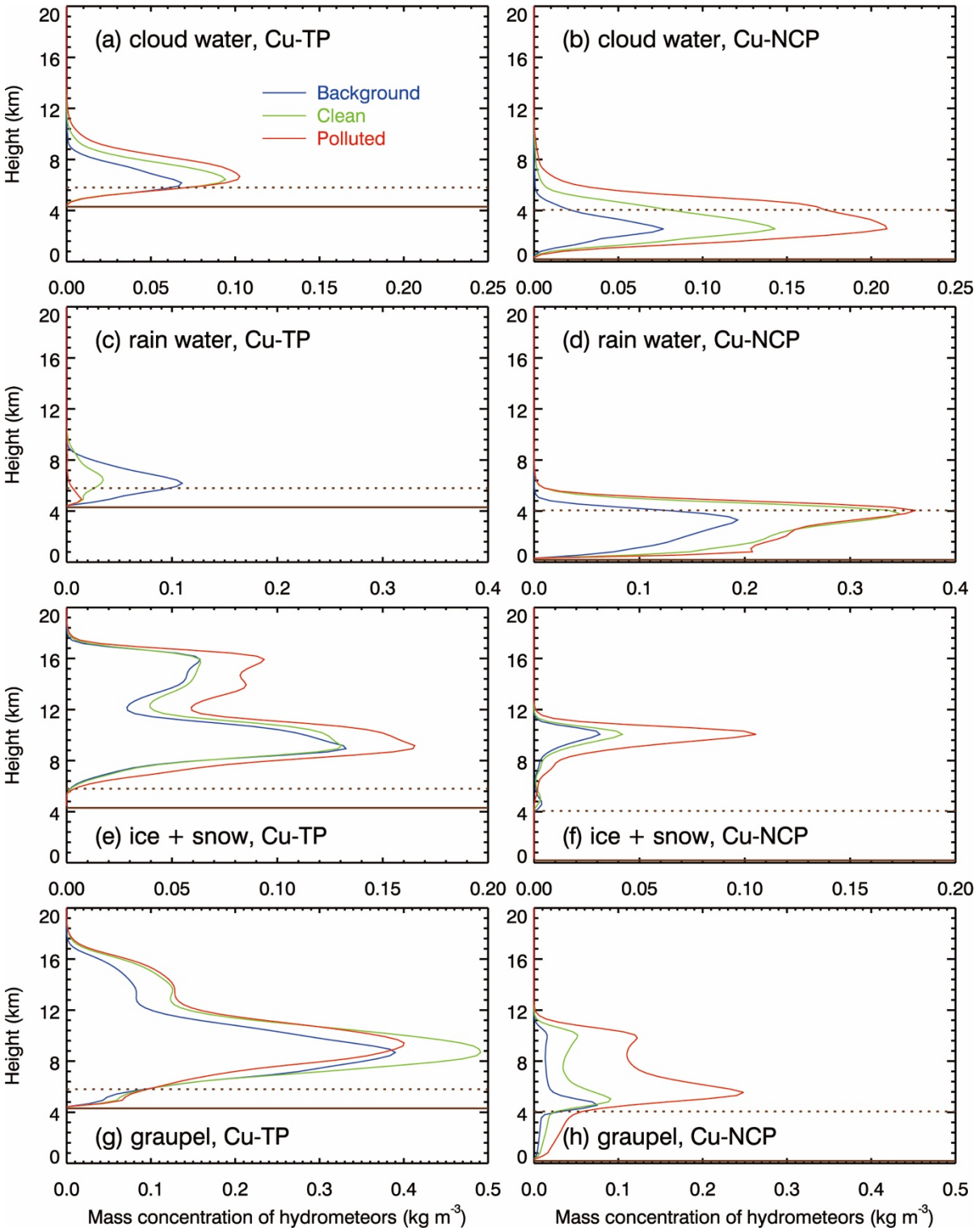

Figure 4 Vertical profiles of time-averaged masses of hydrometeors under background (90 cm^{-3}, blue), clean (900 cm^{-3}, green), and polluted (9000 cm^{-3}, red) [N_a] for (a) and (b) cloud water, (c) and (d) rain water, (e) and (f) ice particles (ice + snow), and (g) and (h) graupel in Cu-TP and Cu-NCP, respectively. The brown solid and dotted lines represent the surface level and the 0°C isotherm, respectively.

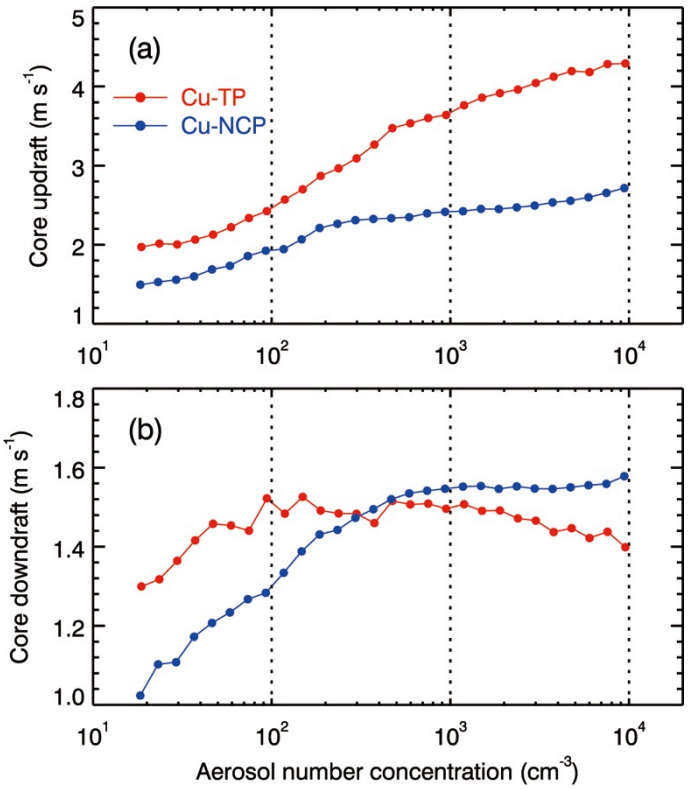

Figure 5 Simulated p-mean of (a) updraft and (b) downdraft in the core area (defined as an area where the absolute vertical velocity of wind is greater than 1 m s^{-1} and the total condensed water content exceeds 10^{-2} g kg^{-1}) as a function of the initial [N_a] in Cu-TP and Cu-NCP.

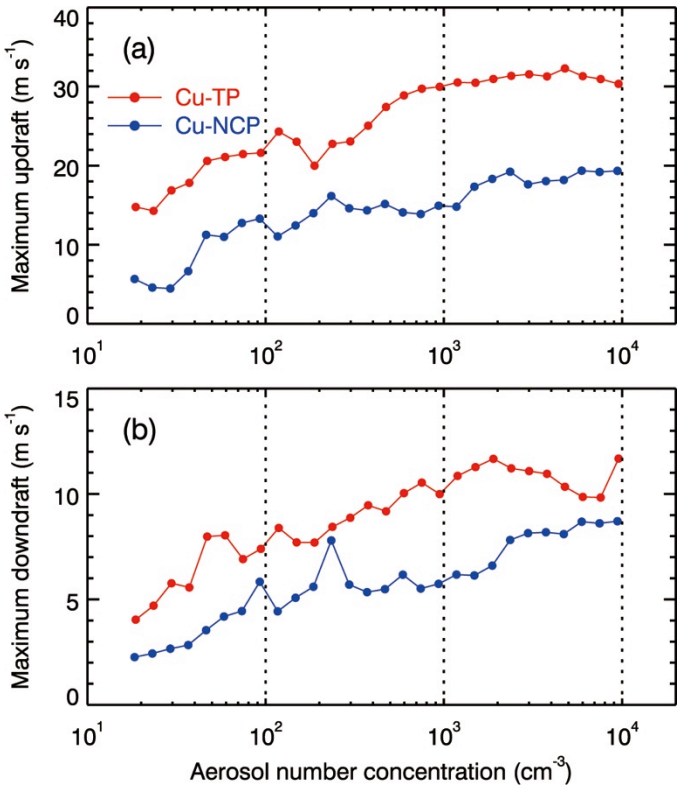

Figure 6 Modeled (a) maximum updraft and (b) minimum downdraft as a function of the initial [N_a] in Cu-TP and Cu-NCP.

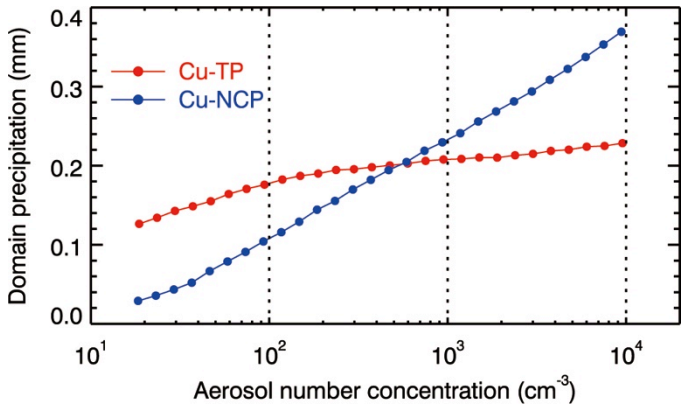

Figure 7 Modeled cumulative precipitation inside the model domain (mm) as a function of the initial [N_a] in Cu-TP and Cu-NCP.

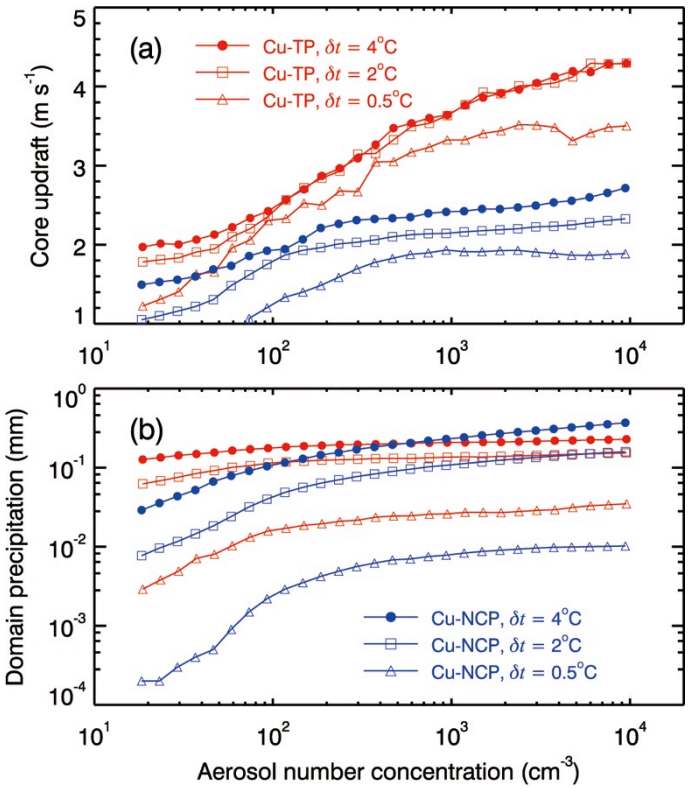

Figure 8 Response of (a) the p-mean of core updraft and (b) cumulative precipitation inside the model domain to the change in the maximum perturbation temperature of the warm bubble under various aerosol conditions in Cu-TP and Cu-NCP.